Multi-immunogenic bioadhesive chitosan-lecithin-podophyllotoxin nanoparticles elicit robust systemic anticancer immunity

Journal:	*SCIENCE CHINA Materials*
Manuscript ID	SCMs-2026-0330.R2
Manuscript Type:	Article
Date Submitted by the Author:	23-Mar-2026

Complete List of Authors:	Zheng, Yun He, Huilan Peng, Yuwei Ye, Chunlian Ji, Jinlong Kong, Xiaotong Zhang, Ying; Soochow University, Zhong, Zhiyuan

Keywords:	chemo-immunotherapy, systemic immune response, immunogenic cell death, multi-immune stimulation, STING activation
Speciality:	Biomaterials

Note: The following files were submitted by the author for peer review, but cannot be converted to PDF. You must view these files (e.g. movies) online.

Figures.rar

Multi-immunogenic bioadhesive chitosan-lecithin-podophyllotoxin nanoparticles elicit robust systemic anticancer immunity

Yun Zheng[a,b], Huilan He[a,b], Yuwei Peng[a,b], Chunlian Ye[b], Jinlong Ji[b], Xiaotong Kong[a], Ying Zhang[a,b]*, Zhiyuan Zhong[a,b,c]*

[a] College of Pharmaceutical Sciences, and State Key Laboratory of Radiation Medicine and Protection, Soochow University, Suzhou, 215123, China

[b] Biomedical Polymers Laboratory, College of Chemistry, Chemical Engineering and Materials Science, Soochow University, Suzhou, 215123, China

[c] International College of Pharmaceutical Innovation, Soochow University, Suzhou, 215123, China

*Corresponding author: yzhang628@suda.edu.cn (Y.Z.); zyzhong@suda.edu.cn (Z.Z.)

ABSTRACT

Chemotherapy-induced immunogenic cell death represents a powerful mechanism to prime systemic antitumor immunity. However, the therapeutic efficacy of conventional chemo-immunotherapies is typically compromised by challenges such as transient immune activation and rapid drug clearance from the tumor site. Herein, we developed chitosan-derived macromolecular immune agonist-functionalized lecithin-podophyllotoxin nanoparticles (CLP-NPs). Unlike traditional inert delivery vehicles, this platform uniquely integrates multivalent agonism with superior bioadhesion, thereby enabling adhesion-mediated retention and sustained multi-engagement with pattern-recognition receptors. By spatiotemporally synchronizing local immunogenic cell death with persistent immune stimulation, this platform effectively converts localized chemotherapy into a robust systemic anticancer immune response. Notably, in a murine MC38 colorectal cancer model, the synergistic combination of CLP-NPs and anti-PD-1 checkpoint blockade therapy elicited a complete regression rate of 83.3% and established potent and long-term immunological memory against tumor recurrence. These findings establish CLP-NPs as a versatile nano-strategy that bridges local cytotoxicity with systemic immune priming, offering a promising translational framework for next-generation chemo-immunotherapies.

Keywords: chemo-immunotherapy, systemic immune response, immunogenic cell death, multi-immune stimulation, STING activation

INTRODUCTION

Chemo-immunotherapy has emerged as a transformative modality in oncology by combining the direct cytotoxic effects of chemotherapy with the capacity of the immune system to establish

durable antitumor surveillance [1, 2]. Certain chemotherapeutic agents, such as anthracyclines and oxaliplatin, can induce immunogenic cell death (ICD) in tumor cells, triggering the release of damage-associated molecular patterns (DAMPs) and tumor-associated antigens (TAAs). These endogenous adjuvants recruit and activate dendritic cells (DCs) to prime antigen-specific $CD8^+$ T lymphocytes [3-6]. Nevertheless, the immune responses triggered by chemotherapy alone are typically transient and localized, rendering them insufficient for complete tumor eradication and long-term recurrence prevention [7-9].

To achieve robust antitumor chemo-immunotherapy, combination strategies integrating chemotherapeutics with exogenous immune agonists have been extensively explored [10-13]. Agonists of pattern-recognition receptors (PRRs), such as Toll-like receptor (TLR), stimulator of interferon genes (STING), and retinoic acid-inducible gene I (RIG-1), initiate strong innate immune signaling cascades to enhance tumor immunogenicity [14-16]. When co-delivered with ICD-inducing agents, these immune agonists augment antigen presentation and increase effector T cell infiltration [17]. Critically, multi-valent constructs characterized by high-density ligands on a polymeric backbone facilitate receptor clustering, which leads to high-avidity engagement and prolonged signaling duration, thereby significantly augmenting the magnitude of adaptive immune responses compared to monovalent ligands [18, 19]. However, strategies that spatiotemporally synchronize multi-valent immune stimulation with localized chemotherapy to overcome the transience of antitumor immunity remain less explored.

Podophyllotoxin (PPT) is a potent microtubule-depolymerizing agent with broad antitumor activity, yet its clinical translation is hindered by poor aqueous solubility, systemic toxicity, and rapid clearance [20, 21]. To address these limitations and augment the therapeutic potency, we developed

tumor-adhesive chitosan-derived macromolecular immune agonist-functionalized lecithin-PPT nanoparticles (CLP-NPs) for synergistic chemo-immunotherapy (**Figure 1**). Unlike conventional inert chitosan-based carriers, the surface-coated CS-5BThi in CLP-NPs acts as a multi-valent immune agonist to provide sustained innate immune stimulation. Meanwhile, the encapsulated PPT serves as a cytotoxic agent to trigger tumor cell apoptosis and initiate ICD, with the lecithin component ensuring stable drug loading. Notably, the cationic structure of CS-5BThi confers superior bioadhesion to the nanoparticles, enabling the adhesion-mediated retention within the tumor microenvironment. By facilitating the spatiotemporal coordination between local chemotherapy and sustained immune activation, CLP-NPs orchestrate potent systemic innate and adaptive immune responses. When combined with anti-PD-1 therapy, CLP-NPs achieved a complete tumor regression rate of approximately 83.3% and established durable immunological memory, offering a versatile and translational framework for advanced chemo-immunotherapies.

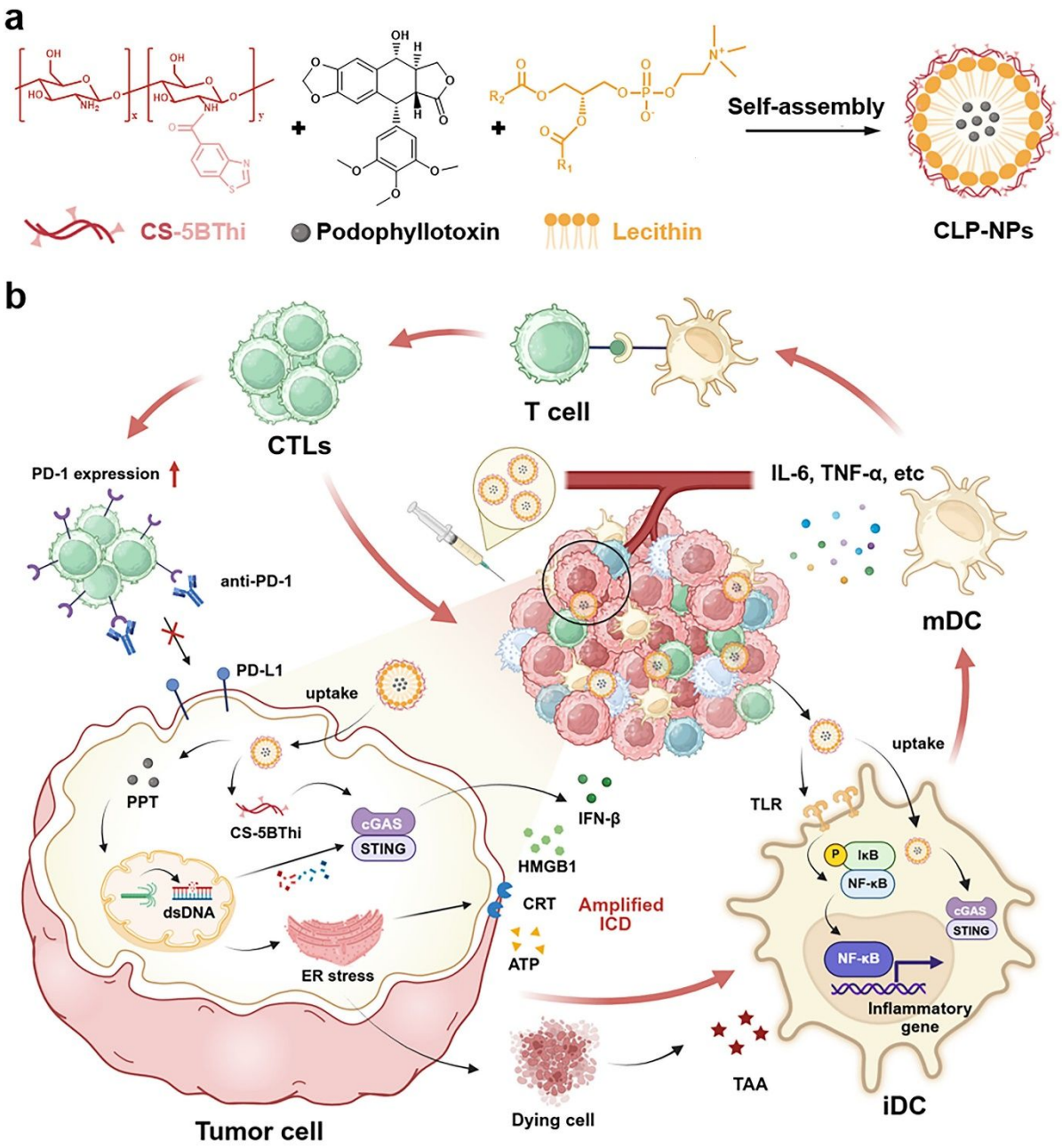

Figure 1. Overview of CLP-NPs preparation and its action on cancer chemo-immunotherapy. **(a)** Schematic illustration of the preparation of CLP-NPs (R_1, R_2: fatty acid residues). **(b)** Overview of the mechanism of action for CLP-NPs in achieving robust and durable cancer chemo-immunotherapy. CLP-NPs exhibit tumor adhesion, potentiate chemotherapy efficacy, and trigger a robust immune response through its multi-valent immune agonist effects. This multi-pronged strategy is further synergized by combination with immune checkpoint inhibitors, thereby offering the promising potential to achieve complete and durable cancer progression.

RESULTS AND DISCUSSION

Design and characterization of multivalent CLP-NPs

To address the poor aqueous solubility and systemic limitations of PPT and to achieve a robust cancer chemo-immunotherapy, we engineered a chitosan-derived multi-valent immune agonist-functionalized lecithin-PPT nanoparticle using a solvent-injection technique (**Figure S1, Supporting Information**). The macromolecular immune agonist (CS-5BThi) was synthesized by tethering chitosan with benzothiazole-5-carboxylic acid as we previously reported [22]. Dynamic light scattering (DLS) analysis and transmission electron microscopy (TEM) revealed that CLP-NPs had a uniform hydrodynamic diameter of approximately 130 nm (**Figure 2a-2b**). Zeta potential measurements demonstrated that LP-NPs exhibited a negative charge, while the incorporation of CS-5BThi confers positive surface charges (**Figure 2c**). These results suggest the surface localization of the chitosan-derived immune agonist, which may not only favor cellular uptake through electrostatic interactions with negatively charged cell membranes but also enable multi-receptor engagement. CLP-NPs demonstrated excellent colloidal stability in both water and phosphate buffer saline (PBS), with negligible changes in particle size and polydispersity index (PDI) (**Figure S2-S3**). However, rapid increase in particle size occurred upon incubation with 10% fetal bovine serum (FBS), likely due to the adsorption of serum proteins by the surface CS-5BThi coating (**Figure S4**). Ultraviolet-visible (UV-Vis) spectroscopy provided evidence of successful PPT encapsulation, as CLP-NPs displayed a broad absorption peak around 280 nm along with a slight hypsochromic shift compared to free PPT (**Figure 2d**). PPT loading was further validated by the characteristic fluorescence spectra of PPT (**Figure 2e**). Encapsulation efficiencies were considerable for both PPT (92.10 ± 0.43%) and chitosan derivative (88.57 ± 2.58%) in CLP-NPs. To elucidate the molecular

interactions involved in CLP-NPs assembly, Fourier transform infrared (FTIR) spectroscopy was performed. As shown in **Figure 2f**, the phosphate group peak shifts from 1251 cm^{-1} (lecithin) to 1238 cm^{-1} (CLP-NPs), and the CS-5BThi-associated band (corresponding to N-H bending vibration) shifts from 1598 cm^{-1} to 1589 cm^{-1} (CLP-NPs). These spectral changes are consistent with alterations in local electronic environment (e.g., electrostatic interaction or hydrogel bonding formation) upon nanoparticle formation.

The release kinetics of PPT from CLP-NPs were evaluated under physiologically relevant pH conditions to simulate the tumor microenvironment and intracellular lysosomal compartments. As shown in **Figure 2g**, CLP-NPs exhibited a pronounced pH-responsive release behavior, with markedly accelerated PPT release under lysosomal pH (5.5) compared to physiological pH (7.4) and mildly acidic pH (6.5). Over 72 h, cumulative PPT release reached approximately 85% at pH 5.5. This behavior may be attributed to the enhanced protonation of CS-5BThi under acidic conditions, which increases the electrostatic repulsion within the CS-5BThi chains, resulting in a loosened surface coating. This structural destabilization facilitates increased permeability of the nanoparticle shell and accelerates drug release in acidic environments. These data suggest that CLP-NPs can preferentially release their payload following endocytic trafficking into acidic tumor lysosomes.

To assess cellular uptake, Cy5-labeled CS-5BThi was incorporated into CLP-NPs and incubated with MC38 colorectal cancer cells. Time-lapse fluorescence analysis revealed pronounced and time-dependent cellular internalization of CLP-NPs (**Figure 2h**). We next evaluated whether CLP-NPs can achieve the co-delivery of CS-5BThi and hydrophobic cargo into the same cells. For this purpose, Coumarin 6 (C6) was used as a hydrophobic fluorescent tracker to replace PPT, and the resulting dual fluorescence-labeled Cy5-CLC6-NPs were examined for intracellular co-localization (**Figure 2i**).

As shown in **Figure 2j**, the strong spatial overlap between C6 and Cy5 signals demonstrated the efficient co-delivery of both functional components into individual cells, which is a prerequisite for their synergistic therapeutic effects.

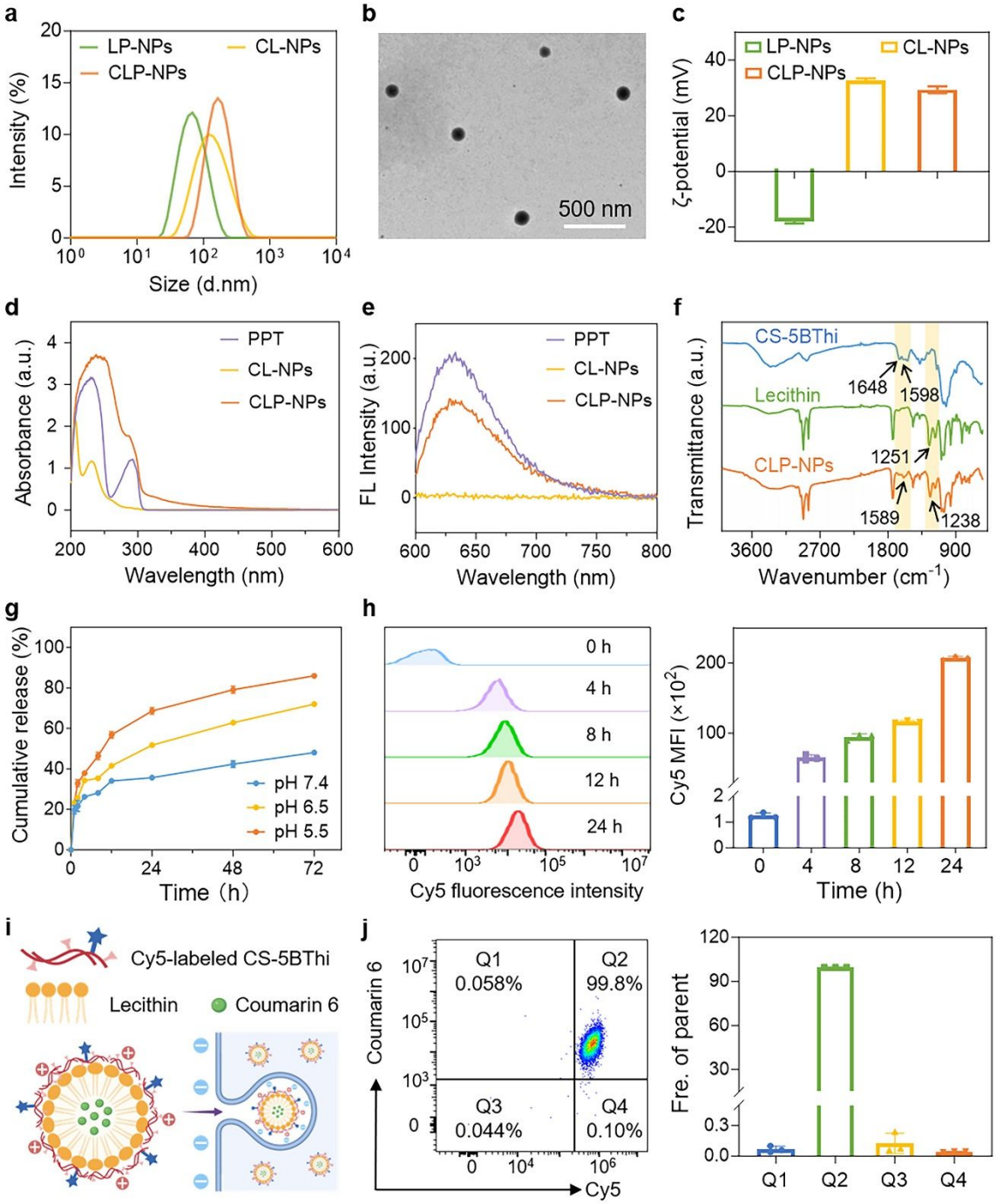

Figure 2. Preparation and characterization of CLP-NPs. **(a)** Size distribution of LP-NPs, CL-NPs and CLP-NPs. **(b)** TEM image of CLP-NPs. **(c)** Zeta potential of LP-NPs, CL-NPs and CLP-NPs (n = 3). **(d)**

UV-vis absorption spectra of PPT, CL-NPs and CLP-NPs in water. **(e)** Fluorescence spectra of PPT, CL-NPs and CLP-NPs in water. **(f)** FTIR spectra of CS-5BThi, lecithin and CLP-NPs. **(g)** Cumulative release profiles of PPT from CLP-NPs at different pH conditions (n = 3). **(h)** Representative histogram graphs of Cy5 fluorescence and the quantitative mean fluorescence intensity (MFI) in MC38 cells after treated with Cy5-labeled CLP-NPs for different time (Cy5 was conjugated on CS-5BThi before CLP-NPs construction; n = 3). **(i)** Schematic illustration of the cellular uptake of Cy5-CLC6-NPs (Cy5 was conjugated on CS-5BThi before CLP-NPs construction; C6 was incorporated into CLP-NPs to substitute PPT). **(j)** Representative flow cytometry analysis of Cy5 and C6 fluorescence and the quantitative co-localization of Cy5 and C6 within MC38 cells after treated with Cy5-CLC6-NPs (n = 3). The data are presented as mean ± SD.

CLP-NPs elicit robust cytotoxicity and amplified ICD

To evaluate the therapeutic potential of CLP-NPs, we initially compared their cytotoxicity against MC38 colorectal cancer cells with that of free PPT and LP-NPs in vitro. As shown in **Figure 3a**, although LP-NPs exhibited cytotoxicity comparable to free PPT, the CLP-NPs formulation demonstrated significantly superior potency across multiple incubation durations. This enhancement is likely due to the improved cellular internalization mediated by the positively charged CS-5BThi moieties on the surface of nanoparticle. Moreover, these surface modifications may facilitate endosomal escape and enable the release of PPT into the cytoplasm, where it can subsequently translocate to the nucleus and exert it antitumor effects [23, 24]. Importantly, the empty CL-NPs exhibited negligible cytotoxicity, confirming the excellent biocompatibility of the delivery system (**Figure 3b**).

PPT exerts its antitumor effects by disrupting microtubule dynamics, ultimately inducing cell cycle

arrest and apoptosis [25]. Flow cytometry analysis revealed that treatment with PPT, LP-NPs, and CLP-NPs all induced G2/M phase arrest in MC38 cells, with CLP-NPs exhibiting the most pronounced effect, arresting 35.32% of cells in the G2/M phase (**Figure S5**). Annexin V/PI staining confirmed that PPT and LP-NPs induced comparable tumor cell apoptosis, while CLP-NPs triggered significantly higher apoptosis rates, with approximately 20% of cells undergoing apoptosis following CLP-NPs treatment (**Figure 3c**). It has been reported that mitotic arrest leads to chromosomal segregation defects, making cells highly prone to DNA double-strand breaks in subsequent cell cycles [26]. To evaluate DNA damage, we quantified the expression of γH2AX, a well-established marker of DNA double-strand breaks. As shown in **Figure 3d**, treatment with PPT, LP-NPs, or CLP-NPs led to significant nuclear fragmentation, with CLP-NPs eliciting the strongest γH2AX signal. These results collectively demonstrate that CLP-NPs enhanced the tumor cell killing efficacy of PPT, amplifying its cytotoxic effects through increased apoptosis and DNA damage.

Beyond direct cytotoxicity, certain chemotherapeutic agents can induce ICD in tumor cells, leading to the release of DAMPs [27, 28]. These DAMPs activate antigen-presenting cells (APCs), facilitate their maturation, and trigger the secretion of pro-inflammatory cytokines, thereby amplifying both innate and adaptive immune responses [29]. CS-5BThi, a multi-valent immune agonist, has been demonstrated with intrinsic immunostimulatory properties that can prime ICD and augment tumor immunogenicity [22]. We hypothesized that the spatiotemporal synchronization of PPT-mediated killing and CS-5BThi-mediated agonism would trigger an amplified ICD cascade. To evaluate the ICD induction, we assessed three well-established markers, calreticulin (CRT), high-mobility group box 1 (HMGB1), and adenosine triphosphate (ATP), expressed by MC38 cells after treated with free PPT or different nanoparticle formulations. Flow cytometry analysis revealed a moderate induction of CRT^{+}

cells after treatment with PPT or LP-NPs, likely due to the anti-mitotic effects of PPT. Notably, a substantial increase in CRT^+ cells was observed following CLP-NPs treatment compared to PBS, PPT and other treatment groups at equivalent component concentrations (**Figure 3e**). Consistently, intracellular HMGB1 levels were significantly decreased in CLP-NPs-treated MC38 cells (**Figure 3f**), indicating its active release and the robust induction of ICD. Moreover, extracellular ATP levels were markedly elevated in the CLP-NPs group compared to other groups (**Figure 3g**). Intriguingly, the remarkable effects of CLP-NPs on tumor cell ICD could not be replicated by a simple mixture of PPT and CL-NPs, highlighting the structural necessity of the integrated nanoplatform (**Figure S6**). These results confirm that the integration of PPT and CS-5BThi into CLP-NPs exhibited synergistic effects in promoting ICD in tumor cells, thereby enhancing their immunogenic potential.

Emerging evidence highlights the pivotal role of the cyclic GMP-AMP (cGAMP) synthase (cGAS)-stimulator of interferon genes (STING) pathway in coordinating antitumor immunity [30, 31]. DNA damage caused by chemotherapeutics can release cytosolic DNA fragments that activate cGAS, leading to the production of cGAMP and downstream STING activation [32, 33]. This cascade ultimately induces type I interferon (IFN-I) production and chemokine secretion (e.g., IFN-β, CXCL10, CCL5) [34]. Given the DNA damage capacities of PPT, we next assessed whether CLP-NPs potentiate cGAS-STING activation. As shown in **Figure 3h**, CLP-NPs treatment significantly upregulated expression of *Ifnβ1*, *Cxcl10* and *Ccl5* in MC38 cells, whereas both PPT alone and LP-NPs induced only modest increase. These findings suggest that the incorporation of CS-5BThi into the nanoparticle elicits substantial immunomodulatory effects, thereby augmenting the immunogenicity of tumor cells and enhancing their susceptibility to immune attack.

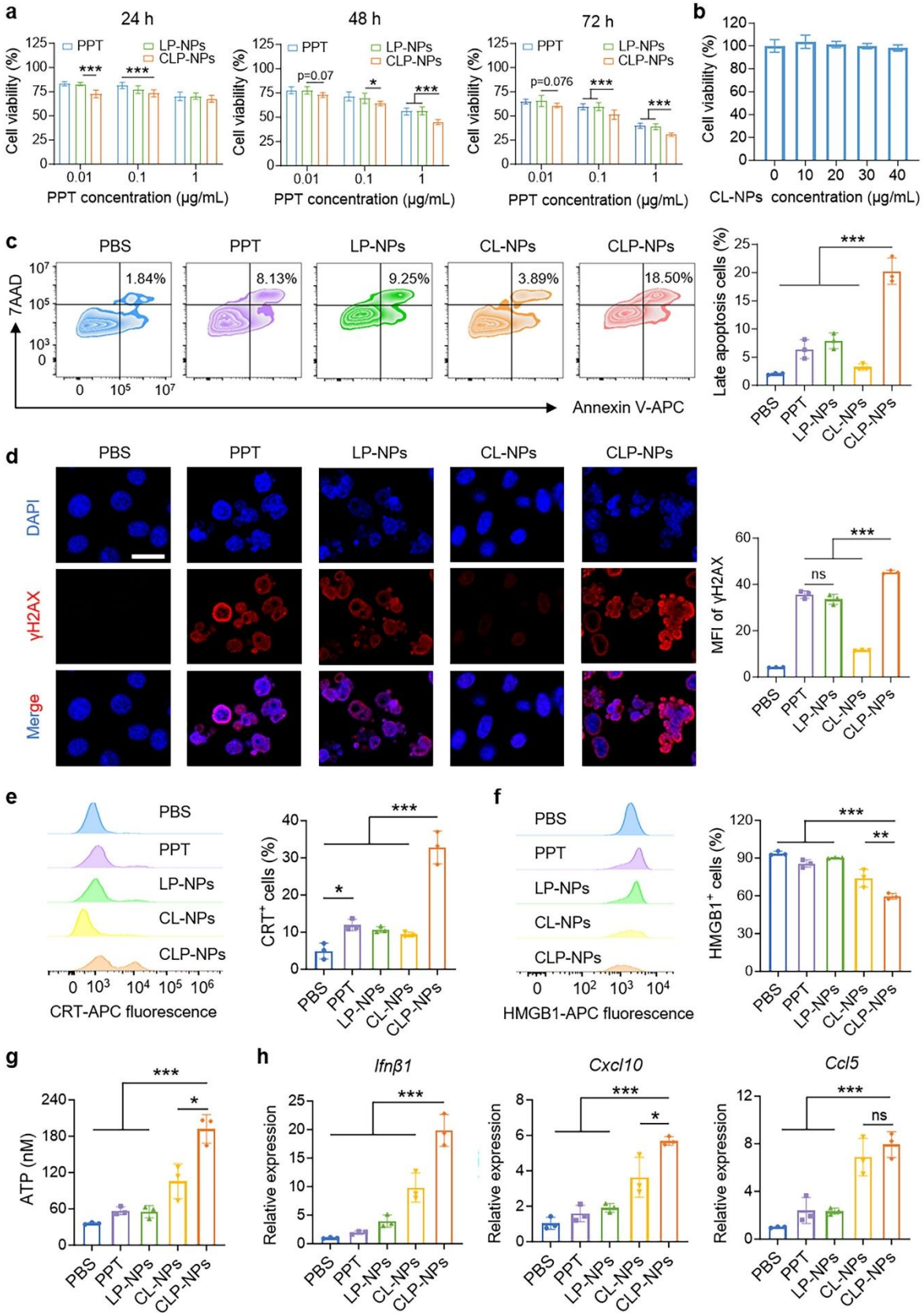

Figure 3. Tumor cell killing and immunogenic effects of CLP-NPs. **(a)** Cell viability of MC38 cells after treated with different concentrations of PPT, LP-NPs or CLP-NPs for different time (n = 6). **(b)** Cell

viability of MC38 cells after treated with different concentrations of CL-NPs (n = 6). **(c)** Representative flow cytometry and quantitative analysis of late apoptosis of MC38 cells after incubated with PPT, LP-NPs, CL-NPs, or CLP-NPs (n = 3). **(d)** Confocal laser scanning microscope (CLSM) images and MFI analysis of the damaged DNA (γH2AX) in MC38 cells after treated with PPT, LP-NPs, CL-NPs, or CLP-NPs (scale bar = 20 μm; n = 3). **(e)** Representative histogram graphs of CRT expression in MC38 cells and the percentages of CRT^+ MC38 cells after different treatment (n = 3). **(f)** Representative histogram graphs of HMGB1 expression in MC38 cells and the percentages of $HMGB1^+$ MC38 cells after different treatment (n = 3). **(g)** Concentrations of ATP in the supernatant of MC38 cell cultures after different treatment (n = 3). **(h)** RT-qPCR analysis of the expression of *Ifnβ1*, *Cxcl10* and *Ccl5* in MC38 cells after different treatment (n = 3). Statistical significance was calculated via two-way ANOVA test in a and one-way ANOVA test in c-h. The data are presented as mean ± SD. *p < 0.05, **p < 0.01, ***p < 0.001.

CLP-NPs stimulate global transcriptomic reprogramming and multi-valent innate immune activation

DCs, as the most potent professional APCs, play a central role in bridging innate and adaptive immunity [35]. Exposure to DAMPs and IFN-Is released from tumor cells during ICD would mature DCs, characterized by upregulation of co-stimulatory molecules and secretion of pro-inflammatory cytokines [36, 37]. To examine whether the ICD induced by CLP-NPs could modulate DC maturation, bone marrow-derived dendritic cells (BMDCs) were co-cultured with the supernatants from MC38 cells pre-treated with different formulations. Flow cytometry analysis revealed that the supernatants from CLP-NPs-treated tumor cells markedly increased the proportion of matured DCs ($CD80^+CD86^+$) from 7.13% to 15.6% (**Figure 4a**).

To further investigate the direct modulation of CLP-NPs on DCs and the underlying molecular pathways, RNA sequencing analysis was performed on BMDCs treated with PBS, PPT, or CLP-NPs. As shown in **Figure S7**, compared to PBS, PPT treatment induced 1,391 differentially expressed genes (708 upregulated and 683 downregulated), while CLP-NPs treatment regulated 3,790 genes (1,556 upregulated and 2,234 downregulated) compared to the PBS group, highlighting the stronger modulatory capacity of CLP-NPs. Kyoto Encyclopedia of Genes and Genomes (KEGG) pathway enrichment analysis of differentially expressed genes revealed that PPT had a limited effect on the activation of the immune pathways in DCs. In contrast, CLP-NPs preferentially enriched genes involved in the cytokine-cytokine receptor interaction and Toll-like receptor signaling pathways, while also activating additional immune pathways, including TNF signaling pathway and JAK-STAT signaling pathway **(Figure 4b)**. Gene set enrichment analysis (GSEA) further demonstrated that CLP-NPs significantly enriched pathways related to interferon-α and interferon-γ responses, inflammatory response, and TNF-α signaling via NF-κB compared to control cells (**Figure 4c**). Heatmap analysis highlighted a robust induction of cGAS-STING-associated genes (e.g., ISGs and IFNs), chemokines, and inflammatory cytokines in BMDCs treated with CLP-NPs **(Figure 4d)**. Consistently, western blot analysis of p-STING, p-TBK1, and p-IRF3 in BMDCs further validated that CLP-NPs effectively primed the cGAS-STING pathway (**Figure S8**). Moreover, studies in murine macrophages demonstrated that while CLP-NPs did not significantly alter polarization, they effectively modulated effector functions by stimulating the secretion of pro-inflammatory cytokines, such as IL6 (**Figure S9**). These results collectively suggest that CLP-NPs not only stimulate immune cells but also elicit a comprehensive transcriptomic reprogramming. By integrating multifaceted immunomodulatory capacities, the CLP-NPs platform effectively remodels the tumor

microenvironment into a highly immunostimulatory niche, thereby supporting the generation of a robust systemic antitumor immunity.

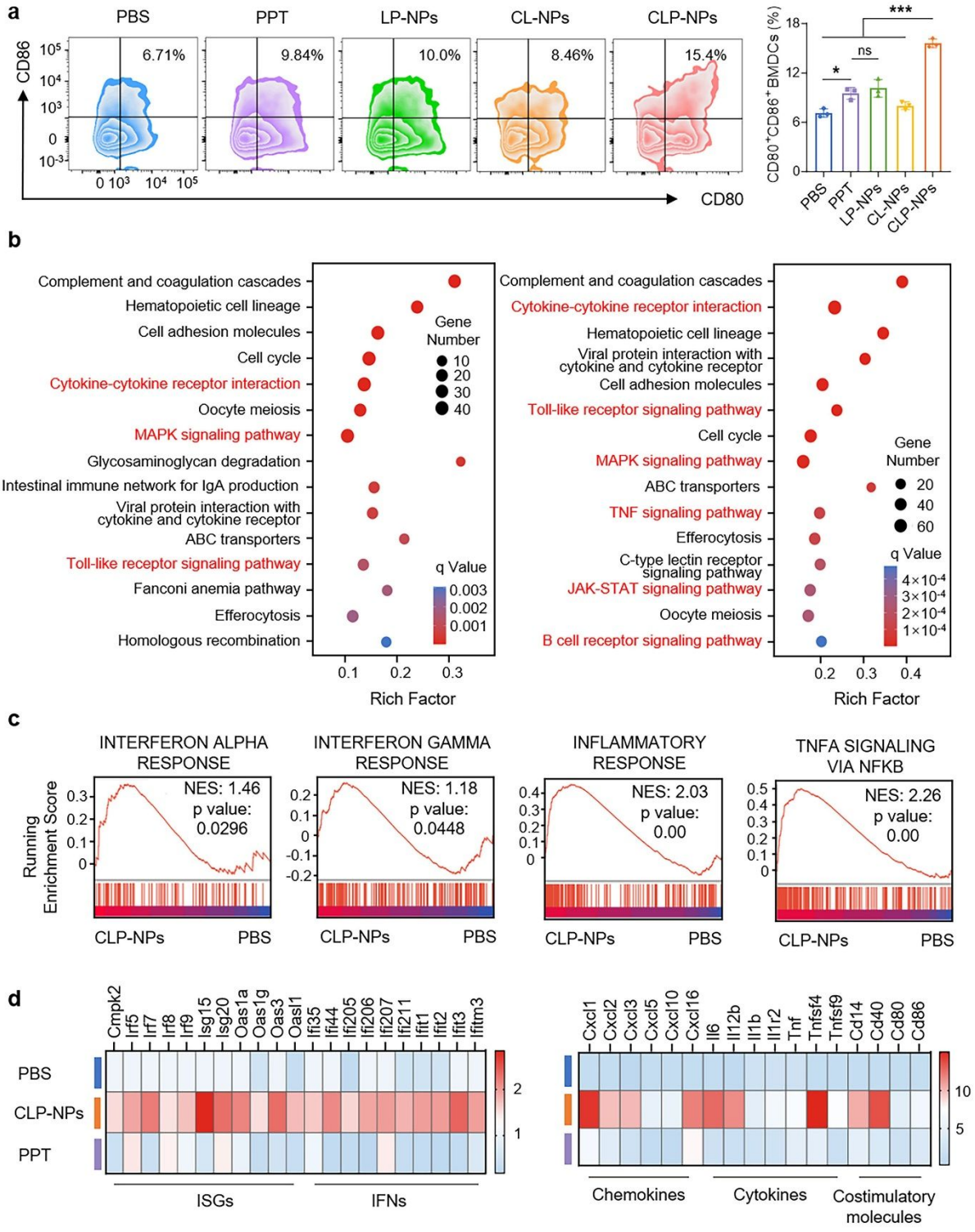

Figure 4. Multi-valent immunostimulatory effects of CLP-NPs on DCs. **(a)** Representative flow cytometry and quantitative analysis of mature BMDCs ($CD80^+CD86^+$) after co-culture with the

supernatants from MC38 cells pre-treated with different formulations (n = 3). **(b)** KEGG pathway enrichment analysis of differentially expressed genes in PPT (left) and CLP-NPs (right) groups. **(c)** GSEA of indicated pathways in CLP-NPs-treated cells. **(d)** Heatmaps of the expression of different genes after treatment. Statistical significance was calculated via one-way ANOVA test. The data are presented as mean ± SD. *p < 0.05, **p < 0.01, ***p < 0.001.

CLP-NPs exhibit prolonged tumor retention and durable antitumor immune protection

Efficient and sustained tumor retention of nanoparticles is critical for localized drug release and durable immune activation. To evaluate the retention of CLP-NPs within tumor tissues, we labeled CS-5BThi with a Cy5 fluorescent dye before nanoparticle construction and administered Cy5-labeled CLP-NPs (Cy5-CLP-NPs) intratumorally into MC38 colorectal cancer-bearing mice. Notably, strong Cy5 fluorescent signals were still observed at the tumor sites three days post-injection of Cy5-CLP-NPs (**Figure 5a-5b**). This sustained retention is attributed to the electrostatic anchoring between the positively charged CS-5BThi motifs and the negatively charged tumor extracellular matrix and cell membranes, which effectively facilitates the adhesion-mediated retention of the nanoparticles. Ex vivo IVIS imaging at 24 h post-injection further revealed that Cy5 fluorescence was predominantly localized within the tumor tissues, with minimal distribution in major organs and tumor-draining lymph nodes (TDLNs) (**Figure S10**). Furthermore, to examine whether CLP-NPs enhance sustained intratumoral retention of hydrophobic drugs, PPT was substituted with Cy5 for CLCy5-NPs construction. Following intratumoral administration, we found that CLCy5-NPs generated markedly stronger and more persistent intratumoral fluorescence signals than free Cy5, highlighting the capacities of nanoparticle architecture to prolong the retention of hydrophobic payloads within tumors (**Figure 5c-5d** and **S11**). We next analyzed the cellular distribution of CLP-NPs within the

tumor microenvironment, which is essential for their immunomodulatory activity. As shown in **Figure 5e**, Cy5-CLP-NPs were internalized by both $CD45^{-}CD31^{-}$ tumor cells and $CD45^{+}$ immune cells. Further analysis revealed that CLP-NPs were effectively internalized by both $CD11c^{+}$ DCs and $CD11b^{+}F4/80^{+}$ macrophages. These results demonstrate that CLP-NPs hold the heterogeneous cellular distribution characteristic, enabling broad interactions across tumor and immune compartments.

Given the potent tumoricidal and immunostimulatory effects of CLP-NPs observed in vitro and their favorable retention and biodistribution in vivo, we next evaluated their therapeutic efficacy in the MC38 colorectal cancer model (**Figure 5f**). Mice bearing established tumors were treated with PBS, free PPT, LP-NPs, CL-NPs or CLP-NPs, and tumor progression and survival were monitored. As illustrated in **Figure 5g-5h** and **S12**, CLP-NPs treatment significantly suppressed tumor growth and prolonged mice survival compared to all control groups. Notably, 66.7% of mice receiving CLP-NPs achieved complete tumor regression, highlighting the superior therapeutic benefit of this chemo-immunotherapeutic strategy. The mice exhibited negligible changes in body weight (**Figure 5i**). These results suggest that the co-delivery of PPT and CS-5BThi synergistically enhances antitumor efficacy beyond that of either agent alone.

To investigate whether the local CLP-NPs treatment elicits systemic immune activation, we analyzed T cell activation markers in peripheral blood. Flow cytometry analyses revealed a marked elevation in CD69 expression on both $CD3^{+}CD8^{+}$ and $CD3^{+}CD4^{+}$ T cells in the CLP-NPs treatment group, indicating robust activation of effector T cells (**Figure 5j-5k**). Additionally, ELISA results revealed significantly increased serum levels of IL-12p70 in the CLP-NPs-treated mice, further suggesting the induction of systemic antitumor immunity (**Figures 5l**). Furthermore, we assessed the durable

immune protection induced by CLP-NPs. Mice with complete tumor regression were re-challenged with MC38 tumor cells on day 90 post-treatment. Strikingly, none of the re-challenged mice developed tumors, whereas naive controls developed progressive disease (**Figure 5m** and **S13**). These findings demonstrate that CLP-NPs not only significantly controlled primary tumors but also orchestrate a long-term immune memory that prevents disease recurrence, highlighting its profound translational potential as a promising chemo-immunotherapeutic platform for refractory cancer eradication.

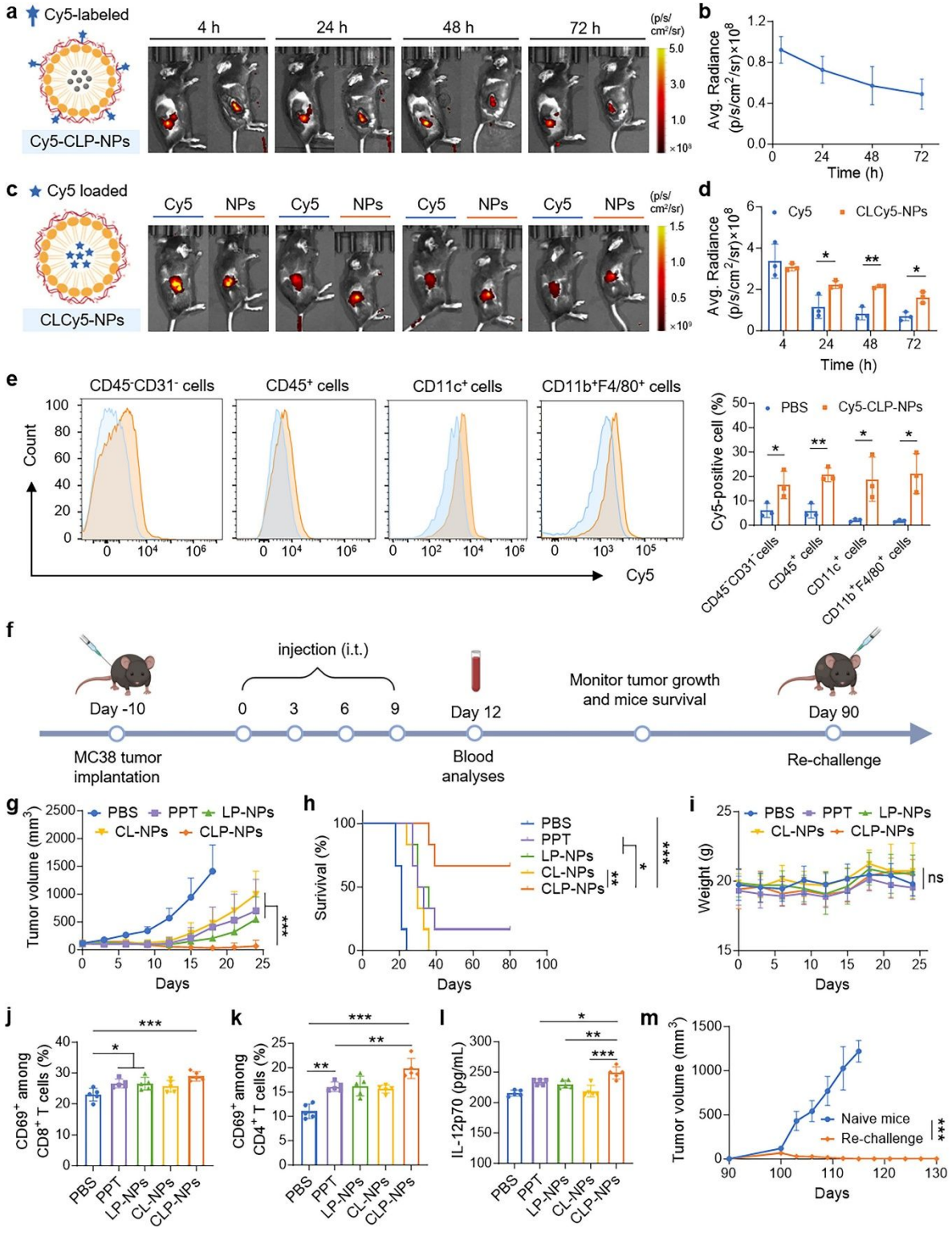

Figure 5. Tumor adhesion and chemo-immunotherapeutic effects of CLP-NPs. **(a)** Schematic illustration of Cy5-CLP-NPs and representative fluorescence imaging of the whole body of MC38 tumor-bearing mice at indicated time points after Cy5-CLP-NPs administration. **(b)** Quantification of

Cy5 fluorescent intensity in tumor sites after Cy5-CLP-NPs administration (n = 3). **(c)** Schematic illustration of CLCy5-NPs and representative fluorescence imaging of the whole body of MC38 tumor-bearing mice at indicated time points after free Cy5 or CLCy5-NPs administration. **(d)** Quantification of Cy5 fluorescent intensity in tumor sites after free Cy5 or CLCy5-NPs administration (n = 3). **(e)** Histogram graphs of Cy5 fluorescence and percentages of Cy5-positive cells among $CD45^-CD31^-$ cells, $CD45^+$ cells, $CD11c^+$ cells, and $CD11b^+F4/80^+$ cells in MC38 tumor tissues (blue lines: PBS; orange lines: CLP-NPs treatment; n = 3). Cy5-CLP-NPs were intratumorally administrated into MC38 tumor-bearing mice 24 h before the analysis. **(f)** Scheme for the antitumor studies on MC38 colorectal cancer-bearing mice. **(g)** Average tumor growth curves after indicated treatments (n = 6). **(h)** Survival rate of mice after indicated treatments (n = 6). **(i)** Average body weight of mice after indicated treatments (n = 6). **(j)** Percentages of $CD69^+$ cells among $CD3^+CD8^+$ T cells in blood (n = 5). **(k)** Percentages of $CD69^+$ cells among $CD3^+CD4^+$ T cells in blood (n = 5). **(l)** Concentrations of IL-12p70 in the serum of MC38 colorectal cancer-bearing mice after indicated treatments (n = 5). **(m)** Average tumor growth curves of re-challenged MC38 colorectal tumors (n = 4). i.t.: Intratumoral. Statistical significance was calculated via multiple comparisons in d and e, two-way ANOVA test in g, the log-rank test in h, one-way ANOVA test in i-l and t-test in m. The data are presented as mean ± SD. $^*p < 0.05$, $^{**}p < 0.01$, $^{***}p < 0.001$.

CLP-NPs combined with anti-PD-1 prime powerful antitumor efficacy

Programmed death receptor 1 (PD-1) is primarily expressed on T cells, while its ligand PD-L1 commonly upregulated on tumor cells and myeloid cells. The binding of PD-L1 to PD-1 can induce T cell apoptosis, dysfunction, and exhaustion, thereby impairing tumor antigen-specific immune responses and enabling tumor immune evasion [38, 39]. Although chemotherapy can induce ICD of

tumor cells, releasing DAMPs to activate DCs and T cells, sustained antigenic stimulation may lead to T cell exhaustion with the inhibitory receptor PD-1 upregulation [40]. Moreover, studies have shown that certain chemotherapeutic agents can also enhance PD-L1 expression on tumor cells via DNA damage response pathways, such as the JAK/STAT signaling cascade, thereby reinforcing an immunosuppressive PD-1/PD-L1 axis [41, 42]. To investigate the impact of CLP-NPs treatment on the PD-1/PD-L1 checkpoint pathway, we examined PD-1 expression on T cells isolated from splenocytes co-cultured with the supernatants of MC38 cells pre-treated with CLP-NPs (**Figure 6a**). As shown in **Figure 6b**, the supernatant from CLP-NPs-pre-treated MC38 cells markedly upregulated PD-1 expression on both $CD3^+CD4^+$ T cells and $CD3^+CD8^+$ T cells. Additionally, tumor PD-L1 expression showed a slight increase post-CLP-NPs treatment (**Figure 6c**). These findings suggest that the combined effects of PPT and CS-5BThi not only enhance tumor cell killing and immunogenicity but also trigger compensatory upregulation of the immune checkpoint PD-1/PD-L1, potentially limiting the duration of immune activation.

Immune checkpoint inhibitors (ICIs) restore immune function by blocking specific inhibitory signals that suppress T cell activation. For instance, anti-PD-1 blocks the interaction between PD-1 on T cells and its ligand PD-L1 on tumor cells or myeloid cells, thereby reactivating T cell effector functions and overcoming tumor immune evasion mechanism [43, 44]. Based on this, we evaluated the therapeutic benefit of combining CLP-NPs with anti-PD-1 in the subcutaneous MC38 colorectal cancer model (**Figure 6d**). As shown in **Figure 6e-6h**, CLP-NPs alone significantly suppressed tumor growth, but their combination with anti-PD-1 produced the strongest efficacy, with 83.3% of mice achieved complete tumor regression. No significant weight loss was observed in any group during the treatment period.

To further evaluate the antitumor immune response priming, multiparametric immune profiling was conducted on day 12. As shown in **Figure 6i**, CLP-NPs + anti-PD-1 combination therapy significantly increased the infiltration of mature DCs in tumors compared to either PBS or CLP-NPs treated mice, suggesting the induction of local antigen processing, which is essential for the downstream adaptive immunity priming. In TDLNs, CLP-NPs and anti-PD-1 combination treatment significantly increased the proportion of both activated $CD8^+$ T cells and $CD4^+$ T cells (**Figure 6j-6k**). Furthermore, in the spleen, the combination treatment significantly elevated the abundance of central memory T cells (Tcm) and effector memory T cells (Tem) within both $CD8^+$ and $CD4^+$ T cell compartments (**Figure 6l** and **S14**), indicating enhanced long-term immune surveillance and the establishment of durable antitumor immune memory. In peripheral blood, although the Tcm levels among $CD8^+$ T cells remained relatively stable after CLP-NPs and anti-PD-1 combination treatment, the proportion of Tem significantly increased (**Figure S15**). This may be attributed to Tcm primarily residing in secondary lymphoid organs, while Tem cells are more widely distributed in peripheral tissues [45] Importantly, histological analysis revealed no significant pathology in major organs (heart, liver, spleen, lung, and kidney) after CLP-NPs and CLP-NPs + anti-PD-1 treatments (**Figure S16**). In summary, combining CLP-NPs and anti-PD-1 effectively overcomes compensatory checkpoint upregulation, promotes DC infiltration, enhances functional memory T cells, and strengthens systemic antitumor immune responses. This combinatorial strategy thus represents a promising chemo-immunotherapeutic paradigm for a powerful and durable tumor control.

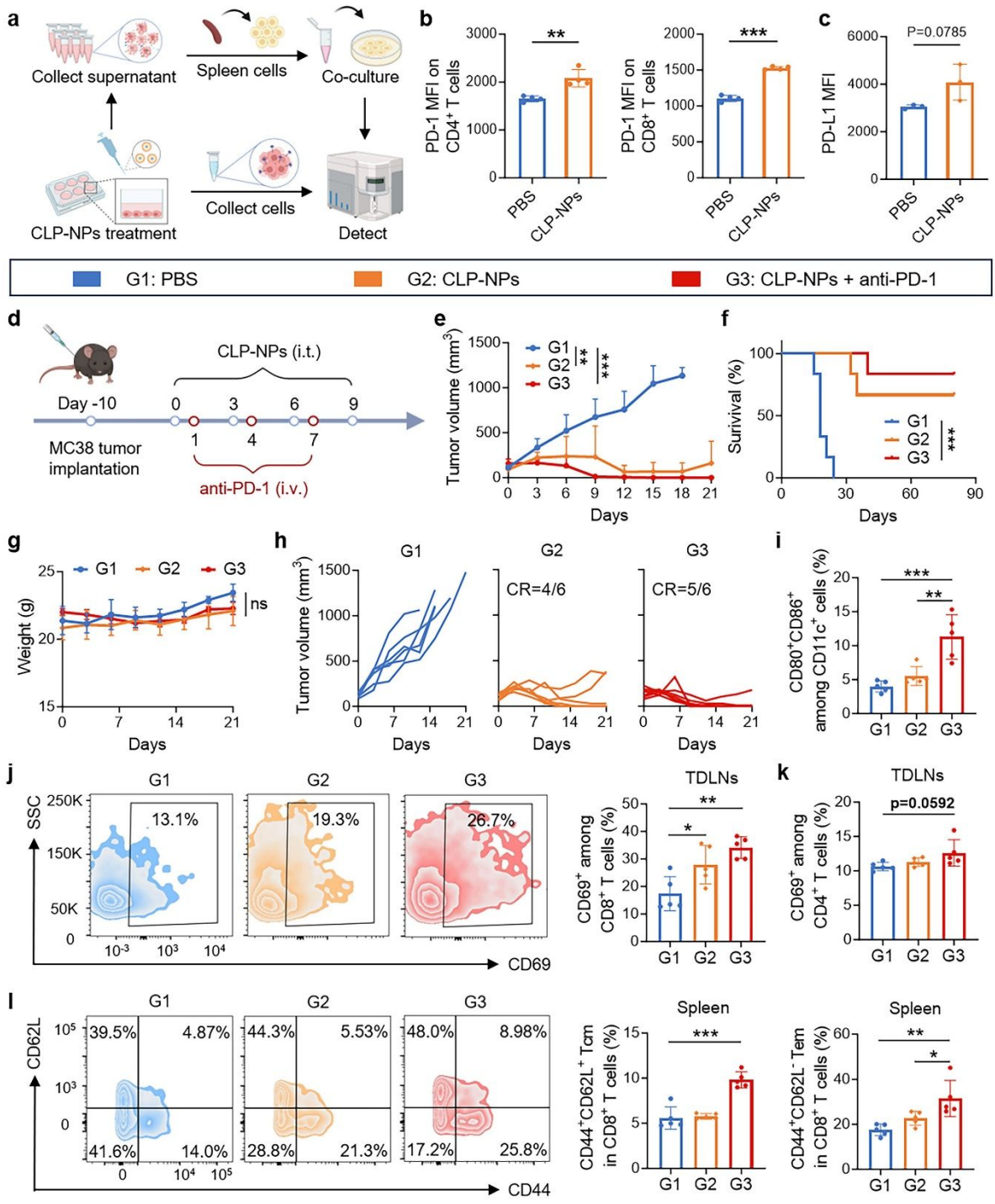

Figure 6. The potency of CLP-NPs in synergizing with anti-PD-1 in cancer therapy. **(a)** Experimental scheme. **(b)** MFI indicated PD-1 expression on $CD4^+$ T cells and $CD8^+$ T cells after splenocytes were co-cultured with the supernatants from MC38 cells pre-treated with CLP-NPs (n = 4). **(c)** MFI indicated PD-L1 expression on MC38 cells after treatment with CLP-NPs (n = 3). **(d)** Scheme for the studies. **(e)** Average tumor growth curves after indicated treatments (n = 6). **(f)** Survival rate of mice

after indicated treatments (n = 6). **(g)** Average body weight of mice after indicated treatments (n = 6). **(h)** Individual tumor growth curves in **(e)**. **(i)** Percentages of $CD80^+CD86^+$ cells among $CD11c^+$ cells in tumor tissues (n = 5). **(j)** Representative flow cytometry analyses and percentages of $CD69^+$ cells among $CD8^+$ T cells in TDLNs (n = 5). **(k)** Percentages of $CD69^+$ cells among $CD4^+$ T cells in TDLNs (n = 5). **(l)** Representative flow cytometry analyses and percentages of $CD44^+CD62L^+$ Tcm and $CD44^+CD62L^-$ Tem among $CD8^+$ T cells in spleen (n = 5). i.t.: Intratumoral. i.v.: Intravenous. Statistical significance was calculated via t-test in b and c, two-way ANOVA test in e, the log-rank test in f, and one-way ANOVA test in g, i-l. The data are presented as mean ± SD. *$p < 0.05$, **$p < 0.01$, ***$p < 0.001$.

CONCLUSIONS

In summary, we have developed CLP-NPs as a spatiotemporally synchronized nano-platform to achieve potent cancer chemo-immunotherapy. By integrating the chemotherapeutic agent PPT with the multi-valent immune agonist CS-5BThi, CLP-NPs effectively bridge direct tumoricidal activity with robust immune priming. The unique bioadhesive properties of this platform enable adhesion-mediated retention, ensuring a prolonged presence within the tumor and facilitating multi-valent engagement with PRRs for sustained immune activation. This strategy not only enhances the therapeutic window of conventional chemotherapy but also successfully remodel the tumor microenvironment, leading to durable tumor control and systemic antitumor immunity in a murine colorectal cancer model. Given its modular design and exceptional therapeutic performance, the CLP-NPs platform represents a promising translational framework for the development of next-generation cancer therapies.

REFERENCES

[1] Schmid D, Sobottka B, Manzo M*, et al.* Tumor immune dynamics and long-term clinical outcome of stage IIIA NSCLC patients treated with neoadjuvant chemoimmunotherapy. Nat Commun, 2025, 16 (1): 8673.

[2] Liu F, Ning S, Wang X*, et al.* Pulsatile sequential drug release system for cascade tumor deep penetration and differentiation therapy to enhance chemoimmunotherapy. Sci Adv, 2025, 11 (36): eadr8001.

[3] Zhang Z, Xu X, Du J, *et al*. Redox-responsive polymer micelles co-encapsulating immune checkpoint inhibitors and chemotherapeutic agents for glioblastoma therapy. Nat Commun, 2024, 15 (1): 1118.

[4] Fan J, Gillespie KP, Mesaros C, Blair IA. HMGB2-induced calreticulin translocation required for immunogenic cell death and ferroptosis of cancer cells are controlled by the nuclear exporter XPO1. Commun Biol, 2024, 7 (1): 1234.

[5] Meier P, Legrand AJ, Adam D, Silke J. Immunogenic cell death in cancer: targeting necroptosis to induce antitumour immunity. Nat Rev Cancer, 2024, 24 (5): 299-315.

[6] Li K, Yu X, Xu Y, *et al.* Cascaded immunotherapy with implantable dual-drug depots sequentially releasing STING agonists and apoptosis inducers. Nat Commun, 2025, 16 (1): 1629.

[7] Sun J, Zheng W, Zhang ZG*, et al.* Selective depletion of tumor-associated SAMHD1 enhances chemotherapeutic efficacy and antitumor immune responses. Signal Transduct Target Ther, 2025, 10 (1): 406.

[8] Patysheva MR, Iamshchikov PS, Fedorenko AA, *et al*. Single-cell transcriptomic profiling of immune landscape in triple-negative breast cancer during neoadjuvant chemotherapy. npj Syst Biol Appl, 2025, 11 (1): 72.

[9] Taniguchi H, Chakraborty S, Takahashi N*, et al.* ATR inhibition activates cancer cell cGAS/STING-interferon signaling and promotes antitumor immunity in small-cell lung cancer. Sci Adv, 2024, 10 (39): eado4618.

[10] Yang Z, Liu H, Li S, *et al*. Temporally programmed STING nanoadjuvant delivery unlocks synergistic chemotherapy-induced antitumor immunity. Sci Adv, 2025, 11 (29): eadw0797.

[11] Zhao K, Yan Y, Jin XK, *et al*. An orally administered gene editing nanoparticle boosts chemo-immunotherapy in colorectal cancer. Nat Nanotechnol, 2025, 20 (7): 935-946.

[12] Au KM, Park SI, Wang AZ. Trispecific natural killer cell nanoengagers for targeted chemoimmunotherapy. Sci Adv, 2020, 6 (27): eaba8564.

[13] Sun Y, Chen W, Sun S, *et al*. Minimalist "in situ" tumor vaccine leveraging versatile dendrimer nanoplatform coordinated ICD and immunoagonist for boosted chemoimmunotherapy. Sci China Mater, 2024, 67 (8): 2700-2708.

[14] Sanlorenzo M, Novoszel P, Vujic I*, et al.* Systemic IFN-I combined with topical TLR7/8 agonists promotes distant tumor suppression by c-Jun-dependent IL-12 expression in dendritic cells. Nat Cancer, 2025, 6 (1): 175-193.

[15] De Leon G, Zhang L, Siddiqui NA*, et al.* An ultrasmall core–shell silica nanoparticle improves antitumour immunity and survival by remodelling suppressive melanoma microenvironments. Nat Nanotechnol, 2026, 21 (2): 311-322.

[16] Chibaya L, DeMarco KD, Lusi CF*, et al.* Nanoparticle delivery of innate immune agonists combined with senescence-inducing agents promotes T cell control of pancreatic cancer. Sci Transl Med, 2024, 16 (762): eadj9366.

[17] Chao Y, Liang C, Tao H*, et al.* Localized cocktail chemoimmunotherapy after in situ gelation to trigger robust systemic antitumor immune responses. Sci Adv, 2020, 6 (10): eaaz4204.

[18] Zhang Y, Liu L, He H, Sun Y, Zhong Z. Dual and multi-immune activation strategies for emerging cancer immunotherapy. Mater Today, 2024, 80: 406-428.

[19] Nam J ,Kim A, Kim K, *et al*. Engineered polysaccharides for controlling innate and adaptive immune responses. Nat Rev Bioeng, 2024, 2 (9): 733-751.

[20] Zhang C, Chen Y, Zuo Y*, et al.* Dual targeting of FR+CD44 overexpressing tumors by self-assembled nanoparticles quantitatively conjugating folic acid-hyaluronic acid to the GSH-sensitively modified podophyllotoxin. Chem Eng J, 2025, 505: 159276.

[21] Xiang Y, Wang B, Yang W, *et al*. Mitocytosis mediated by an enzyme-activable mitochondrion-disturbing polymer-drug conjugate enhances active penetration in glioblastoma therapy. Adv Mater, 2024, 36 (18): 2311500.

[22] He H, Liu L, Zheng Y, *et al*. Tumor-adhesive chitosan-derived multi-immune agonist unleashes strong and durable anti-cancer immunity. Adv Sci, 2025, 12 (16): e2414110.

[23] Zhang J, Hu Y, Wen X*, et al.* Tandem-controlled lysosomal assembly of nanofibres induces pyroptosis for cancer immunotherapy. Nat Nanotechnol, 2025, 20 (4): 563-574.

[24] Zhu Y, Xu W, Chen W, *et al*. Self-assembling peptide with dual function of cell penetration and antibacterial as a nano weapon to combat intracellular bacteria. Sci Adv, 2025, 11 (6): eads3844.

[25] Lin Z, Wang Y, Li W, *et al*. A natural compound-empowered podophyllotoxin prodrug nanoassembly magnifies efficacy-toxicity benefits in cancer chemotherapy. Asian J Pharm Sci, 2024, 19 (4): 100892.

[26] Zhang W, Liu S, Hou Y, *et al*. Functional nanoplatform for modulating cellular forces to enhance antitumor immunity via mechanotransduction. J Control Release, 2025, 379: 850-865.

[27] Liu Y, Zhang G, Li Q*, et al.* Nano-assemblies overcome cancer multidrug resistance for effectively synergistic chemo-immuno-oncotherapy. Chem Eng J, 2024, 490: 151437.

[28] Cen Y, Chen Y, Cai H, *et al*. Carrier-adjuvanted immunostimulator to boost photodynamic immunotherapy by downregulating PD-L1 and impairing ATP hydrolysis. Sci China Mater, 2025, 68 (2): 626-639.

[29] Hu P, He S, Tian H. Organic semiconducting polymers for cancer sonodynamic immunotherapy. Polym Sci Technol, 2026, 2: 22-39.

[30] Wilson JT. Controlling the STING pathway to improve immunotherapy. Nat Nanotechnol, 2024, 19 (6): 718-720.

[31] Wang Q, Yu Y, Zhuang J, Liu R, Sun C. Demystifying the cGAS-STING pathway: precision regulation in the tumor immune microenvironment. Mol Cancer, 2025, 24 (1): 178.

[32] Wang W, Yang F, Zhang L, *et al*. Targeting DNA damage and repair machinery via delivering WEE1 inhibitor and platinum (IV) prodrugs to stimulate STING pathway for maximizing chemo-immunotherapy in bladder cancer. Adv Mater, 2024, 36 (1): e2308762.

[33] Qing Y, Hu P. DNA damage activates cGAS-STING pathway facilitating NK cell recognition and clearance of T-cell acute lymphoblastic leukemia. Blood, 2024, 144 (Supplement 1): 7188-7188.

[34] Han J, Hu S, Hu Y*, et al.* Discovery of podofilox as a potent cGAMP-STING signaling enhancer with antitumor activity. Cancer Immunol Res, 2023, 11 (5): 583-599.

[35] Wang H, Li H, Wang X, Ding J. Immunologically effective chiral polymers to potentiate anti-cancer immune responses. Polym Sci Technol, 2025, 1 (10): 809-811.

[36] Xu X, Wang R, Li D*, et al.* Guanidine-modified nanoparticles as robust BTZ delivery carriers and activators of immune responses. J Control Release, 2023, 357: 310-318.

[37] Li X, Gao ML, Wang SS, *et al*. Nanoscale covalent organic framework-mediated pyroelectrocatalytic activation of immunogenic cell death for potent immunotherapy. Sci Adv, 2024, 10 (48): eadr5145.

[38] Lin X, Kang K, Chen P, *et al*. Regulatory mechanisms of PD-1/PD-L1 in cancers. Mol Cancer, 2024, 23 (1): 108.

[39] Ying W, Zheng C, Gong C*, et al.* Nanorobots hold PD-L1 and break membrane of colorectal cancer cells for

immunotherapy. Nat Nanotechnol, 2026, 21: 156-167.

[40] Pandit M, Kil YS, Ahn JH*, et al.* Methionine consumption by cancer cells drives a progressive upregulation of PD-1 expression in CD4 T cells. Nat Commun, 2023, 14 (1): 2593.

[41] Li Y, Wang J, Yu R, *et al*. Leveraging chemotherapy-induced PD-L1 upregulation to potentiate targeted PD-L1 degradation using nanoparticle-based targeting chimeras. Chem Eng J, 2024, 499: 155708.

[42] Chen R, Li Z, Fang Z, *et al*. Chemotherapy-mediated induction of PD-L1 via SEI1 facilitates myeloma immune evasion. Adv Sci, 2025, 12 (19): 2411082.

[43] Liu Y, Xie Y, Chen Y*, et al.* A protease-cleavable liposome for co-delivery of anti-PD-L1 and doxorubicin for colon cancer therapy in mice. Nat Commun, 2025, 16 (1): 2854.

[44] Liang J, Fang Y, Wu B, *et al*. Harnessing self-assembling peptides on γδ T cells to enhance anti-tumor immunity. Polym Sci Technol, Doi: 10.1021/polymscitech.5c00053.

[45] Zhao X, Hu W, Park SR, *et al*. The transcriptional cofactor Tle3 reciprocally controls effector and central memory CD8+ T cell fates. Nat Immunol, 2024, 25 (2): 294-306.

Acknowledgments

This work was financially supported by the National Natural Science Foundation of China (52573171, 52303199, 52233007), Suzhou Innovation and Entrepreneurship Leading Talent Plan (ZXL2025330), and the Natural Science Foundation of the Jiangsu Higher Education Institutions of China (23KJB350006).

Author Contributions

Y. Zheng, Y. Zhang, and Z. Zhong conceived the project; Y. Zheng, H. He, Y. Peng, and C. Ye performed the experiments and analyzed the data; J. Ji, and X. Kong provided technical input on this project; Y. Zheng, Y. Zhang, and Z. Zhong drafted the manuscript; Y. Zhang and Z. Zhong supervised the project.

Conflict of interest

Y. Zheng, Y. Zhang and Z. Zhong have filed a patent on the chitosan-lecithin-podophyllotoxin nanoparticles. The other authors declare no competing financial interest.

Table of content

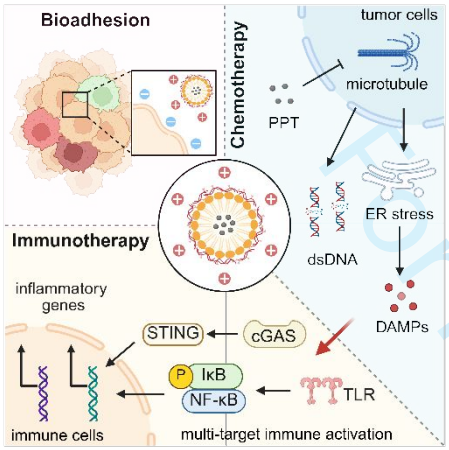

多重免疫原性生物粘附型壳聚糖-卵磷脂-鬼臼毒素纳米粒诱导强效系统性抗肿瘤免疫

郑云 [a,b], 何绘蓝 [a,b], 彭雨薇 [a,b], 叶春莲 [b], 吉金龙 [b], 孔晓彤 [a], 张滢 [a,b*], 钟志远 [a,b,c*]

化疗诱导的免疫原性细胞死亡是启动系统性抗肿瘤免疫应答的重要机制。然而，传统的化疗-免疫联合治疗往往受到免疫激活持续时间短及肿瘤部位药物清除过快等因素的限制。针对这些问题，我们开发了一种新型壳聚糖衍生的大分子免疫激动剂功能化卵磷脂-鬼臼毒素纳米粒（CLP-NPs）。不同于传统的惰性递送载体，该平台将多价免疫激动作用与优异的生物黏附特性相结合，通过黏附介导的滞留效应，实现了对模式识别受体的持续多点作用。通过在时空层面协同调控局部免疫原性细胞死亡与持续的免疫刺激，该体系能够有效将局部化疗转化为强有力的系统性抗肿瘤免疫反应。实验结果表明，在小鼠 MC38 结直肠癌模型中，CLP-NPs 联合 anti-PD-1 免疫检查点阻断治疗可实现高达 83.3% 的肿瘤完全消退率，并诱导持久的免疫记忆以抑制肿瘤复发。本研究提出的 CLP-NPs 纳米策略在局部细胞毒性与系统性免疫启动之间建立了有效连接，为下一代化疗-免疫联合治疗的临床转化提供了新的思路。

Yun Zheng received her B.S. degree from Yanbian University in 2023. Her research focuses on the development of immune adjuvants for cancer immunotherapy.

Ying Zhang is an associate professor at Soochow University. She received her PhD from Changchun Institute of Applied Chemistry, Chinses Academy of Sciences, in 2019. Her research interests include cancer radioimmunotherapy and the development of novel immune adjuvants.

Zhiyuan Zhong is a professor at Soochow University. He received his PhD from University of Twente in 2002. His research focuses on controlled drug release (including chemotherapeutics, proteins, nucleic acid drugs, and radiopharmaceuticals), targeted cancer therapy, and cancer immunotherapy.